Quantitative GITT analysis of a model system with applications to lithium-sulfur batteries

James W. Dibden[a], Nina Meddings[a], John R. Owen[a] and Nuria Garcia-Araez*[a]

Abstract: Galvanostatic Intermittent Titration Technique (GITT) is a powerful characterization tool for batteries that provides key thermodynamic and kinetic information about battery performance. However, the quantitative analysis of GITT measurements of lithium-sulfur batteries has so far been limited to the evaluation of the internal resistance of the cell and the equilibrium voltage profiles. In this work, we provide the mathematical framework to characterize the mass transport kinetics in lithium-sulfur batteries from GITT data and we demonstrate the validity of the approach via the application to a model and well-behaved system, ethyl viologen, whose diffusion coefficient is corroborated by cyclic voltammetry. The present approach is also advantageous for the analysis of ion-insertion electrodes, where non-linearity of concentration and voltage changes would produce unrealistic evaluations of the diffusion coefficient by the classical analysis of GITT data.

Introduction

Galvanostatic Intermittent Titration Technique (GITT) is an electrochemical technique that involves the application of a series of current pulses, each followed by a relaxation period where no current passes through the cell. A mathematical framework for the quantitative analysis of GITT data was demonstrated in 1977 by Weppner and Huggins,[1] who showed that the technique could be used to characterize the transport kinetics and thermodynamics in ion-insertion electrodes. The rate of ion transport in the bulk of the electrode is often the rate-determining step, and because of that, GITT has been extensively applied to evaluate the ambipolar diffusion coefficient of lithium, which ultimately determines the battery rate capability.

The application of GITT to lithium-sulfur batteries can potentially provide a rich set of information about the reaction mechanism, the timescales of the different steps and the unusual properties of the concentrated polysulfide solutions formed in-situ in lithium-sulfur batteries. GITT measurements have already been used to evaluate the internal resistance of lithium-sulfur cells, demonstrating that cell failure is associated to a rapidly increasing resistance.[2,3] GITT has also been used to obtain the (quasi) equilibrium voltage of the cells and it has also been shown that GITT data can be used to demonstrate qualitative differences in the rate of different processes involved in lithium-sulfur cell reactions, for cells made with different electrolytes, different electrodes or operated at different temperatures.[4-8] However, a quantitative analysis of GITT data to evaluate transport kinetics is still missing. This is because of the complexity of lithium-sulfur battery reactions, which makes the mathematical approach developed by Weppner and Huggins[1] unsuitable for these batteries.

The following characteristics of lithium-sulfur batteries make the approach by Weppner and Huggins for ion-insertion electrodes inapplicable:

1) Redox reactions in lithium-sulfur batteries take place in the liquid state, and transport of species takes place in solution, as opposed to the situation of solid state ion diffusion within an insertion electrode.

2) A variety of polysulfide species are formed during the operation of lithium-sulfur batteries, which sometimes coexist with solid sulfur and/or solid Li_2S.

3) Polysulfides can shuttle from the sulfur electrode to the lithium electrode, producing battery self-discharge.

In this work, we demonstrate the use of GITT measurements to characterize the transport kinetics of species in solution. We validate the mathematical derivation by using a model, well-behaved electrochemical system (ethyl viologen (II), EtV^{2+}). The diffusion coefficient of EtV^{2+} in an electrolyte typical of lithium-sulfur batteries (1 M LiTFSI in 1,3-dioxolane) is evaluated by cyclic voltammetry. It is shown that our analysis of GITT data provides values of diffusion coefficient that are consistent with cyclic voltammetry, while using the simplified approach proposed by Weppner and Huggins leads to marked inconsistencies. Therefore, the approach here developed is suitable to characterize the rate of transport of soluble species such as sulfur or polysulfides in lithium-sulfur batteries, as well as the rate of transport of the electron-lithium ion pair in one-phase lithium insertion materials. The complications associated with having solid sulfur and/or Li_2S present in the battery will be addressed in future work. In all the experiments presented here, shuttling of species from the working electrode to the counter/reference electrode is avoided via the introduction of a lithium-ion conductive glass ceramic membrane (LICGC, Ohara Corporation).

This work is a first step towards the application of GITT to the more complex Li-S battery, and complements other approaches to unravel the fundamental redox and diffusion properties of the complex polysulfide solutions formed in Li-S cells. For example, a detailed analysis of impedance measurements of polysulfide solutions with well-behaved glassy carbon electrodes, complemented with UV-vis measurements, demonstrated the importance of disproportionation reactions, and the use of this technique to estimate values of the relevant rate constants and diffusion coefficients.[9] Impedance spectroscopy has also been used to evaluate the individual contributions from electrolyte resistance, charge transfer, ion diffusion and electrode surface layers,[10-15] which in turn has been used to refine mechanistic models of Li-S cells,[16,17] as well as to investigate capacity fading.[18-20] Other experimental techniques used to elucidate redox and diffusion properties in Li-S cells include XAS,[21-32] in-operando optical imaging of the temporal and spatial distribution

[a] Mr. J. W. Dibden, Ms. N.C. Meddings, Prof. J.R. Owen, Dr. Nuria Garcia-Araez
Chemistry
University of Southampton
University Road, Highfield, Southampton SO17 1BJ
E-mail: N.Garcia-Araez@soton.ac.uk

of polysulfides,[33] UV-Vis spectroscopy,[34-42] NMR,[43-46] EPR/ESR,[40,47] XRD,[48-55] Raman,[56-60] HPLC,[61-64] and gas evolution,[65] among other electrochemical studies.[66-68] The mechanism and kinetics of Li_2S precipitation has been studied using chronoamperometry.[69] In terms of the shuttle behavior of polysulfides, methods to experimentally quantify the rate of the shuttle process have been proposed, as well as models of the process and its effect on capacity, charge efficiency and self-discharge.[70-73] Indeed, there have been efforts to model the behavior of Li-S cells more generally, including the effect of reaction kinetics and transport properties.[74-78] In this work, we demonstrate a reliable method to determine the mass transport kinetics of soluble species, and such information can be used to validate and complement the other techniques. The advantages of GITT is that it can be applied to practical cells and provides an evaluation of the diffusion coefficient that does not require prior knowledge of the speciation (number of electrons involved in the reaction) or concentration of species.

This article is organized as follows. First, an evaluation of the diffusion of ethyl viologen (II) in the chosen solvent (1 M LiTFSI in 1,3-dioxolane) by cyclic voltammetry is presented in section 1. Then, the mathematical background required for the analysis of GITT is explained in section 2. The results and discussion of GITT data is presented in section 3. Full experimental details are provided at the end of the article.

Results and Discussion

1. Evaluation of the diffusion coefficient of ethyl viologen (II) by cyclic voltammetry

Figure 1 shows cyclic voltammograms measured at different scan rates at a glassy carbon electrode in a solution containing 5 mM $EtV(OTf)_2$ in 1 M LiTFSI in 1,3-dioxolane. The voltammograms show the characteristic duck-shape of a reversible electrochemical system with fast electron transfer.[79] The cathodic peak corresponds to the reduction of EtV^{2+} to EtV^{+}, and the anodic peak to the oxidation of EtV^{+} to EtV^{2+}. These measurements were done in a Swagelok cell containing a glass-embedded glassy carbon electrode. The glassy carbon electrode was separated from the counter/reference electrode by glass fiber separators soaked in the electrolyte. Therefore, the measurements accurately reflect the rate of mass transport of ethyl viologen (II) in the electrolyte-soaked separator. This allowed a quantitative comparison with the analysis of the GITT data, which was also obtained in a Swagelok cell containing ethyl viologen (II) present in the electrolyte-soaked glass fiber separator.

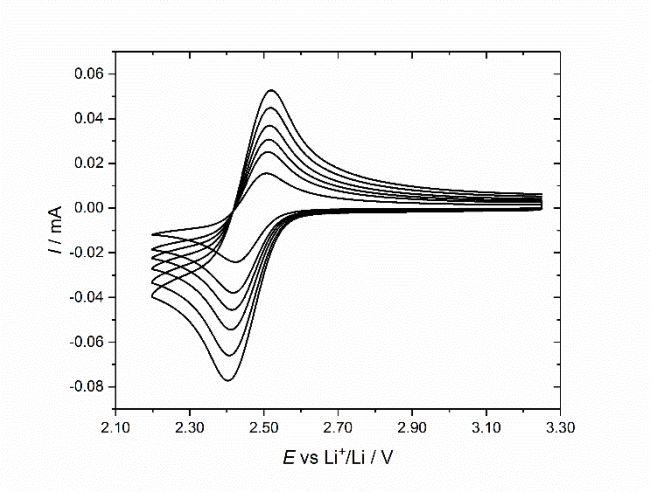

Figure 1. Cyclic voltammograms recorded at a glassy carbon electrode in a Swagelok cell containing three glass fiber separators soaked in 5 mM $EtV(OTf)_2$ + 1 M LiTFSI in 1,3-dioxolane.

Figure 2 shows the plot of peak potentials vs. peak current for the EtV^{2+} to EtV^{+} process, as obtained from the data in figure 1 at different scan rates. Extrapolation to zero current shows a difference of peak potentials of 69 mV, in reasonable agreement with the 59 mV expected for a fully reversible system. Therefore, the Randles-Sevcik equation was used to evaluate the value of the diffusion coefficient from the peak current:

$$I_p = 2.69 \cdot 10^5 n^{3/2} A D^{1/2} c\, v^{1/2} \qquad (1.1)$$

where I_p is the peak current, n is the number of electrons, A is the electrode area, D is the diffusion coefficient, c is the concentration and v is the scan rate. Note that the constant in the Randles-Sevcik equation equals $2.69 \cdot 10^5$ C mol^{-1} V$^{-0.5}$.

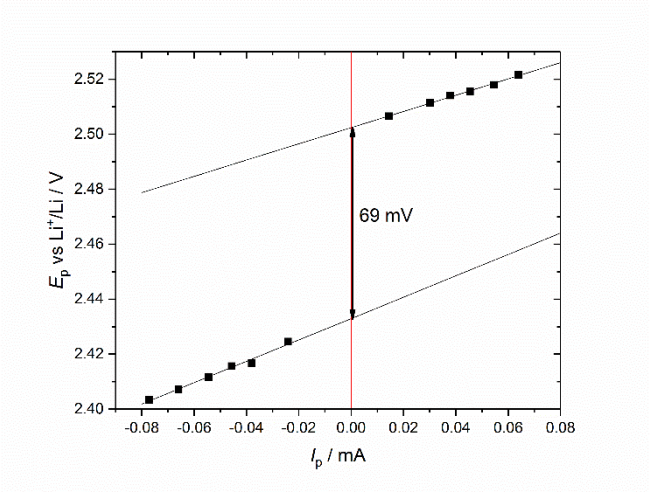

Figure 2. Plot of peak potential against peak current for the measurements shown in figure 1.

Figure 3 shows the plot of peak current vs. the square of the scan rate. The slope of the plot gives a value of diffusion coefficient of $3.2 \cdot 10^{-6}$ cm^2 s^{-1} for EtV^{2+} in the electrolyte soaking the glass fiber separator. An average value of $(2.8 \pm 0.4) \cdot 10^{-6}$ cm^2 s^{-1} was obtained upon repetition of these measurements. The formal standard potential of the EtV^{2+}/EtV^{+} process, $E^{0'}$ =2.46 V vs. Li^+/Li, has also been obtained from the average in peak potential of the cathodic and anodic processes:

$$E^{0'} = \frac{E_{pc} + E_{pa}}{2} \qquad (1.2)$$

where E_{pc} and E_{pc} are the cathodic and anodic peak potentials, as extrapolated to zero current from figure 2.

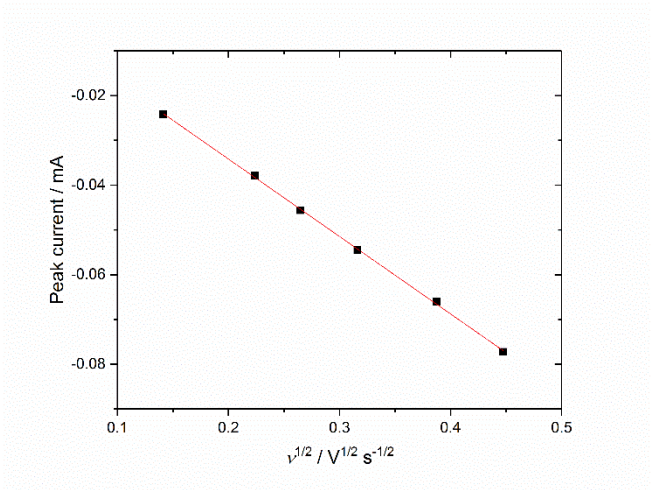

Figure 3. Plot of peak potential against the square room of the scan rate, for the measurements shown in figure 1.

In order to improve the accuracy of the analysis of voltammetric data, the measurements in figure 1 were done without a lithium conductive membrane separating the working and counter-reference electrodes (only glass fiber separators were placed in between the two electrodes). In this way, the internal cell resistance of the cell was relatively small (150 Ω), despite the small area of the glassy carbon electrode (0.07 cm^2), and hence the effect of the IR correction was also small, <12 mV. The counter-reference electrode in those experiments was a partially de-lithiated $LiFePO_4$ electrode, $Li_{0.5}FePO_4$, which has a constant potential of 3.45 V vs. Li^+/Li. EtV^{2+} is stable in contact with this electrode (80). EtV^{+} is oxidized to EtV^{2+} by $Li_{0.5}FePO_4$, but the effect of that reaction on the voltammograms in figure 1 is negligible, since the EtV^{+} is only created at the surface of the glassy carbon working electrode, and the time for EtV^{+} to diffuse to the $Li_{0.5}FePO_4$, electrode is around L^2/D (where L is the thickness of the three glass fibers separators used in these experiments, ca. 0.1 cm), which is >1 hour.

2. Background for the GITT analysis

GITT involves the application of a series of current pulses, each of them followed by a long relaxation step, and this sequence of current pulse + relaxation step is usually repeated many times until the battery is fully charged or discharged. The current pulse produces a change in concentration of the redox species according to Fick's first law:

$$\frac{I_0}{A} = -nFD_O\left(\frac{\partial c_0}{\partial x}\right)_{x=0} = nFD_R\left(\frac{\partial c_R}{\partial x}\right)_{x=0} \qquad (2.1)$$

where I_0 is the applied current, A is the electrode area, n is the number of electrons, F is Faraday's constant, D_O and D_R are the diffusion coefficients of oxidized and reduced species, respectively, and c_O and c_R are the concentrations, and x is the distance from the electrode surface. The variation of the surface concentrations induced by the current pulse is given by (79):

$$c_O^{x=0} = c_O^{initial} - \frac{2I_0\sqrt{t}}{AnF\sqrt{D_O\pi}} \qquad \left(t << \frac{L^2}{D}\right) \qquad (2.2a)$$

$$c_R^{x=0} = c_R^{initial} + \frac{2I_0\sqrt{t}}{AnF\sqrt{D_R\pi}} \qquad \left(t << \frac{L^2}{D}\right) \qquad (2.2b)$$

where t is time, and $c_O^{initial}$ and $c_R^{initial}$ are the initial concentrations of oxidized and reduced species before each pulse. Figure 4b illustrates the calculation of the variation of the surface concentrations during one pulse, using the conditions of the experiments presented in section 3. The surface concentrations are plotted against the square root of time, and therefore the plots are linear, as expected from equation (2.2). Figure 4c shows the calculation of the electrode potential during the current pulse, as obtained using the Nernst equation:

$$E = E^{0'} + \frac{RT}{nF}\ln\frac{c_O^{x=0}}{c_R^{x=0}} \qquad (2.3)$$

where it is considered that all activity coefficients are unity. Note that the experimental potential will show an additional constant shift due to the IR drop, as illustrated in figure 4c. It is observed that the variation of the potential with the square root of time is not linear, which is the main problem with the application of the classical analysis of GITT data. This point will be discussed in more detail.

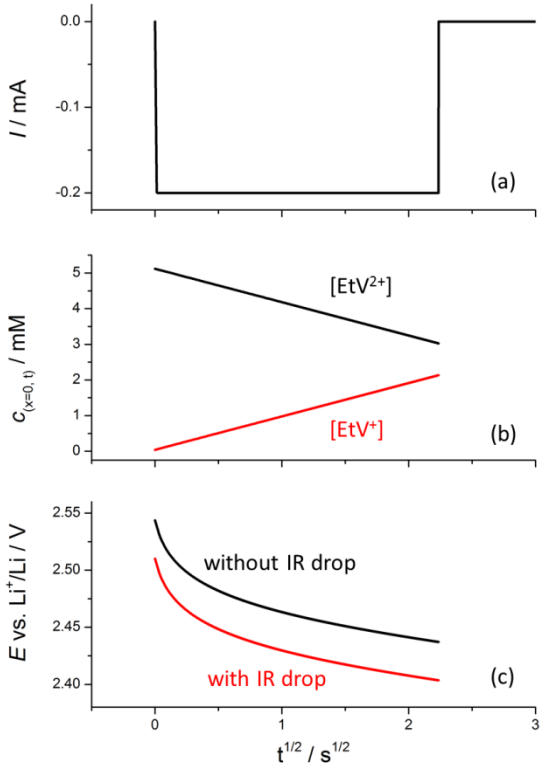

Figure 4. Plot of applied current (a), calculated surface concentrations of EtV^{2+} and EtV^{+} (b) and calculated electrode potential, with and without *IR* drops (c), against the square room of time. Calculations have been done using equations (2.2 and 2.3) for the experimental conditions corresponding to the 2nd pulse in the GITT measurements in figure 6 (calculations of the 1st pulse are less accurate since only trace amounts of EtV^{+} are present initially in the cell): I^0 = 0.2 mA, A = 1.77 cm^2, n=1, $D_O = D_R = 3{\cdot}10^{-6}$ cm^2 s^{-1}, $c_O^{initial}$ = 5.11 mM, $c_R^{initial}$ = 0.04 mM. The duration of the pulse is 5 seconds. The *IR* drop has been included considering R=168 Ω, as found experimentally in the GITT data.

Equation (2.2) is only applicable for current pulse durations shorter than L^2/D, where L is the thickness of the media where concentration profiles develop and D is the diffusion coefficient. In the present case, L is the electrolyte thickness, which equals the thickness of the two glass fiber separators used in the present GITT measurements. L^2/D provides an estimation of the time involved in the diffusion of species with diffusion coefficient D over a distance L. Once species reach the other side of the separator, they will be affected by the boundary condition established between the electrolyte-soaked separator and the lithium-ion conductive glass membrane that is placed after it. Since the flux of viologen species is blocked by the lithium-ion conductive membrane, the concentration gradient should be zero. As a result the evolution of the concentration profiles will be disturbed by this additional boundary condition, and equation (2.2) will not hold.

Figure 5 illustrates the concentration profiles at the end of the 1st and 84th pulse using the following equation (79):

$$c_O = c_O^{x=0} - \frac{I^0}{nFAD_O}\left[2\sqrt{\frac{D_O t}{\pi}}\,exp\left(-\frac{x^2}{4D_O t}\right) - x\,erfc\left(\frac{x}{2\sqrt{D_O t}}\right)\right] \quad \left(t \ll \frac{L^2}{D}\right) \qquad (2.4)$$

At the end of the pulses, the concentration profiles have reached their maximum spread. Thus, figure 5 shows that, for the pulse duration of 5 seconds employed here, the changes in concentration during the current pulses take place within 0.01 cm from the electrode surface, which is much shorter than the thickness of the separator used in the present GITT measurements (two glass fiber separators: $L \approx 0.07$ cm when fully compressed). This is because the duration of the pulse is much shorter than L^2/D, which is around 40 minutes. Figure 5 also shows that the analysis of the GITT data from pulse 84 onwards should be done with more care, since the surface concentration of the oxidized species effectively reaches zero during the current pulse. For the case under study, this will mean that EtV^{2+} will be converted to EtV^{+}, which will then be converted to EtV^{0} towards the end of the current pulse. Careful inspection of the experimental results presented in section 3 shows that the effect of conversion of EtV^{+} to EtV^{0} is already noticeable from around the 75th pulse onwards. This could be due to small misalignment of the electrodes or to a small overestimation of the diffusion coefficient in the application of equation 2.4 (using $D=2{\cdot}10^{-6}$ cm^2 s^{-1} it is found that the surface EtV^{2+} concentration drops to zero at the end of pulse 74).

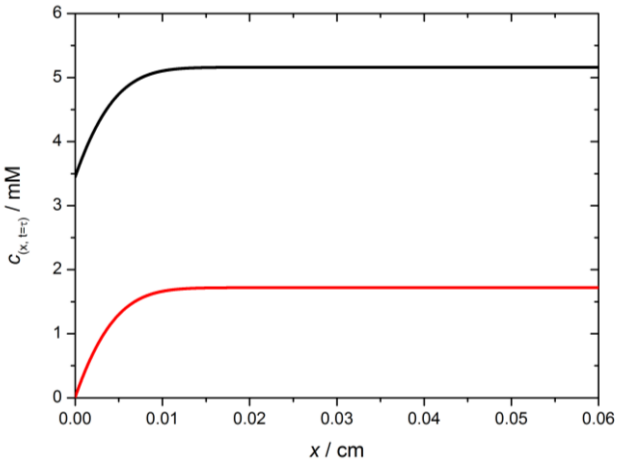

Figure 5. Calculated EtV^{2+} concentration as a function of the distance from the electrode, at the end of the 1st and 84th pulse in GITT measurements, using equation (2.4). All parameters as in figure 4.

When the change in surface concentration induced by the current pulse is small, Weppner and Huggins (1) proposed that the change in potential would be proportional to the change in concentration:

$$\Delta E_{PULSE} = k\Delta c_{PULSE} \qquad (2.5)$$

where k is a proportionality constant, $\Delta E_{PULSE} = E_{initial} - E_{PULSE}$ where $E_{initial}$ is the potential before the pulse and E_{PULSE} is the potential during the pulse (without IR contributions), and $\Delta c_{PULSE} = c_{initial} - c_{PULSE}$ is the change in oxidized or reduced species concentration. According to equation (2.2), and considering for simplicity $D_O = D_R = D$:

$$\Delta c_{PULSE} = \frac{2I_0\sqrt{t}}{AnF\sqrt{D\pi}} \qquad \left(t << \frac{L^2}{D}\right) \qquad (2.6)$$

The proportionality constant *k* can be obtained experimentally from the change in the equilibrium potential at the end of the relaxation:

$$\Delta E_{RELAX} = k \Delta c_{RELAX} \quad (2.7)$$

where $\Delta E_{RELAX} = E_{initial} - E_{RELAX}$, and $\Delta c_{RELAX} = c_{initial} - c_{RELAX}$. E_{RELAX} and c_{RELAX} are the values of potential and concentration at the end of the relaxation. ΔE_{RELAX} can be obtained from experiments and Δc_{RELAX} can be calculated with Faraday's law:

$$\Delta c_{RELAX} = \frac{\tau I_0}{n\, F\, V_{electrolyte}} \quad (2.8)$$

where τ is the duration of the current pulse and $V_{electrolyte}$ is the volume of electrolyte (250 µl in the present measurements). Combining equations (2.5-2.8), the following expression of the change in potential during the current pulse can be obtained:

$$\Delta E_{PULSE} = \Delta E_{RELAX} \frac{2 V_{electrolyte}}{\tau\, A} \sqrt{\frac{t}{D\pi}} \qquad \left(t << \frac{L^2}{D} \right) \quad (2.9)$$

Thus, the change in potential at the end of the pulse, when t = τ , will be:

$$\Delta E_{PULSE}^{t=\tau} = \Delta E_{RELAX} \frac{2 V_{electrolyte}}{A\sqrt{\tau D \pi}} \qquad \left(t << \frac{L^2}{D} \right) \quad (2.10)$$

And the diffusion coefficient can be obtained from

$$D = \left(\frac{4}{\tau\pi} \right) \left(\frac{V_{electrolyte}}{A} \right)^2 \left(\frac{\Delta E_{RELAX}}{\Delta E_{PULSE}^{t=\tau}} \right)^2 \qquad \left(t << \frac{L^2}{D} \right) \quad (2.11)$$

Note that equation (2.11) only holds if equation (2.9) holds for the whole duration of the pulse, as pointed out by Weppner and Huggins.[1] This can be checked, in principle, by plotting ΔE_{PULSE} vs. $\sqrt{t}$ and checking the linearity of the plot. However, deviations at short times will always be observed due to the formation of an IR drop as the current changes from zero (before the pulse) to a constant value (during the pulse). At longer times, deviations can also be observed as the concentration profiles spread over a distance greater than the thickness of the separator, which means that the condition of $t << \frac{L^2}{D}$ does not hold. More importantly, deviations can also be observed at longer times when the change in concentration and the change in potential are not proportional, as required by equation 2.7. Despite these complications, it is possible, in principle, to obtain an accurate evaluation of the diffusion coefficient, provided that the plot of ΔE_{PULSE} vs. $\sqrt{t}$ is linear at intermediate times, by using the value of the slope of the plot, $d\Delta E_{PULSE} / d\sqrt{t}$:

$$D = \left(\frac{4}{\pi} \right) \left(\frac{V_{electrolyte}}{\tau A} \right)^2 \left(\frac{\Delta E_{RELAX}}{d\Delta E_{PULSE} / d\sqrt{t}} \right)^2 \quad (2.12)$$

However, in practice, ascertaining the linearity of plot of ΔE_{PULSE} vs. $\sqrt{t}$ is rather subjective and dependent on how the plot is made. We will show here that unphysical values of the diffusion coefficient can be obtained, with unphysical variations of the magnitude of the diffusion coefficient of over two orders of magnitude.

It will be shown that a more accurate analysis of GITT data can be done using the Nernst equation in order to establish the relationship between concentrations and potential. In this way, the variation of potential during the pulse can be obtained by combining equations 2.2 and 2.3:

$$\Delta E_{PULSE} = \frac{RT}{nF} \ln \frac{c_O^{initial} - \dfrac{2 I_0 \sqrt{t}}{AnF\sqrt{D_O \pi}}}{c_O^{initial}} - \frac{RT}{nF} \ln \frac{c_R^{initial} + \dfrac{2 I_0 \sqrt{t}}{AnF\sqrt{D_R \pi}}}{c_R^{initial}} \qquad \left(t << \frac{L^2}{D} \right) \quad (2.13)$$

where $c_O^{initial}$ and $c_R^{initial}$ are the concentrations of oxidized and reduced species before the current pulse, which can be obtained by taking into account the initial concentration of species and the change in concentration induced by previous pulses, which is given by equation (2.8).

3. Analysis of GITT data

Figure 6 shows the results of the GITT measurements of a cell containing 5 mM EtV^{2+} in the working electrode compartment, which is separated from the counter-reference electrode by a lithium-ion conductive glass membrane (Ohara). From pulse 75 onwards, the variation of the potential during the pulses is much greater than in earlier pulses. This is due to depletion of EtV^{2+} at the electrode surface (see figure 5), which results in the transition from the EtV^{2+} to EtV^{+} conversion to the EtV^{+} to EtV^{0} process, which takes place at around 2 V vs. Li^+/Li. In the following, the analysis will be focused on the first 75 pulses, where this complication does not take place.

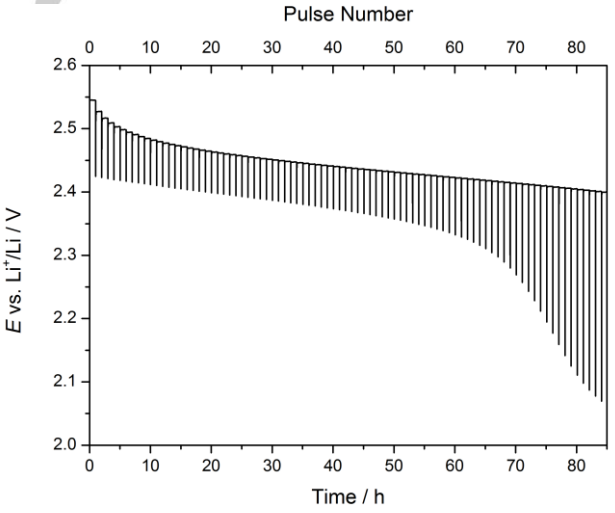

Figure 6. GITT measurements of a cell containing two glass fiber separators soaked in 5 mM $EtV(OTf)_2$ + 1 M LiTFSI in 1,3-dioxolane in the working electrode compartment with a carbon coated aluminium foil working electrode, a lithium-ion conductive glass membrane (LICGC, Ohara Corporation), and one glass fiber separator soaked in 1 M LiTFSI in 1,3-dioxolane with lithium metal as counter-reference electrode. In each pulse, a current of 0.11 mA cm^{-2} was applied for 5 s, followed by a rest period of 1 hour. All experimental parameters are the same as in the calculations in figures 4-5 and 7-8.

In each pulse, a fraction of EtV^{2+} is converted into EtV^{+}. At the end of each of the relaxation steps, the concentrations of EtV^{2+} and EtV^{+} have equilibrated within the separator in the working electrode compartment, and the cell voltage reaches a steady-state potential which corresponds to the equilibrium potential of the cell. The experimental steady-state potential can be compared with the calculation of the equilibrium potential using the Nernst equation:

$$E = E^{0'} + \frac{RT}{F}\ln\frac{[\mathrm{EtV}^{2+}]_{RELAX}}{[\mathrm{EtV}^{+}]_{RELAX}} \qquad (3.1)$$

where $[\mathrm{EtV}^{2+}]_{RELAX}$ and $[\mathrm{EtV}^{+}]_{RELAX}$ are the equilibrium concentrations of EtV^{2+} and EtV^{+} at the end of the relaxation, and they are calculated using Faraday's law, taking into account that in each pulse, the change in concentration is given by equation (2.8). Under the present conditions Δc_{RELAX} is around 0.04 mM (that is, each pulse produces a decrease in $[EtV^{2+}]$ of 0.04 mM and an increase in $[EtV^{+}]$ of 0.04 mM). The state of charge (SOC) of the cell can be defined as:

$$SOC = \frac{\text{moles of } \mathrm{EtV}^{+}}{\text{moles of } \mathrm{EtV}^{2+} + \text{moles of } \mathrm{EtV}^{+}} = \frac{[\mathrm{EtV}^{+}]_{RELAX}}{[\mathrm{EtV}^{2+}]_{RELAX} + [\mathrm{EtV}^{+}]_{RELAX}} \qquad (3.2)$$

where $[\mathrm{EtV}^{2+}]_{RELAX}$ + $[\mathrm{EtV}^{+}]_{RELAX}$ equals the initial ethyl viologen concentration (5 mM in the present case). Figure 7 compares the experimental and calculated equilibrium potentials as a function of the state of charge of the cell, evidencing an excellent agreement.

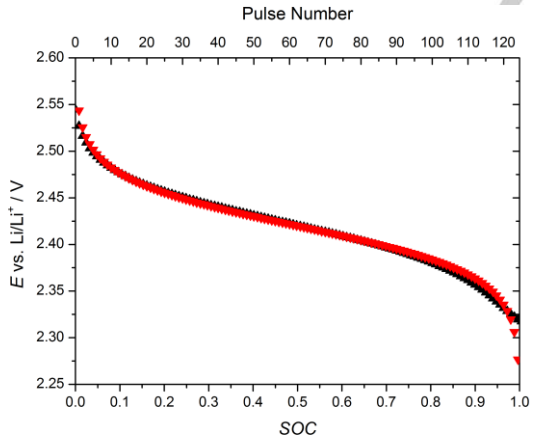

Figure 7. Comparison of equilibrium potential values as obtained experimentally from the GITT measurements in figure 6 (black) and from calculation using the Nernst equation (equation 3.1, red). All parameters for the calculation are taken directly from the experimental values, and the value of E^0 = 2.42 V vs. Li^+/Li has been used, in good agreement with voltammetric experiments, which give E^0 = 2.46 V vs. Li^+/Li.

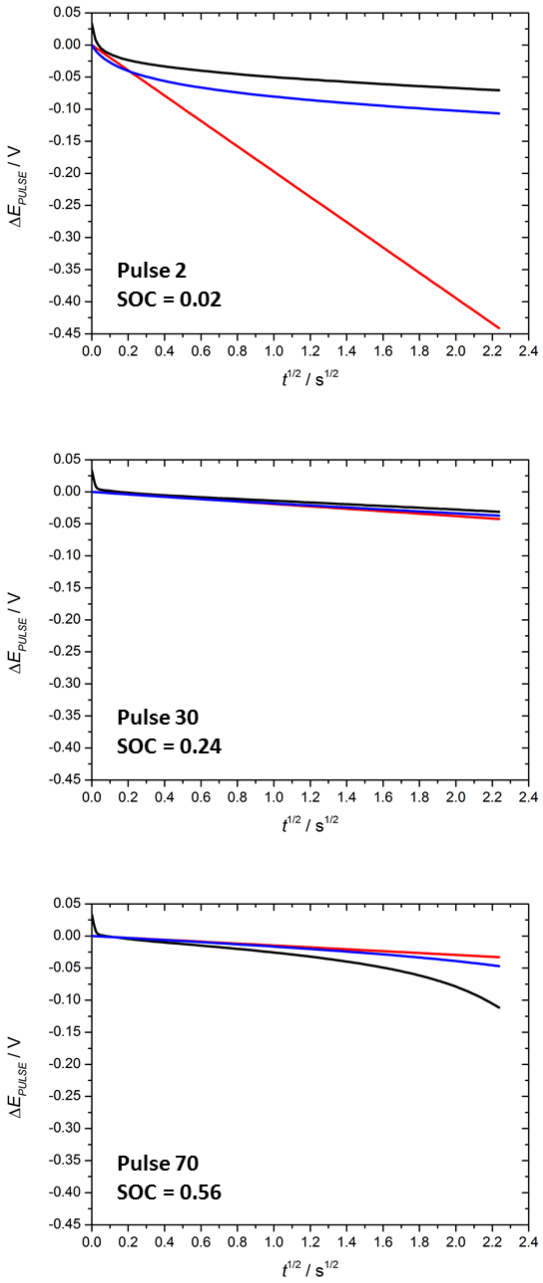

Figure 8. Comparison of experimental (black) and calculated (red: using equation 2.9, blue: using equation 2.13) values of the change in potential induced by the current pulse, for the pulse number indicated. All parameters for the calculations have been taken directly from the experimental values, and D = $3\cdot10^{-6}$ cm^2 s^{-1} has been used, in agreement with the analysis of voltammetric data, which give D = $(2.8 \pm 0.4)\cdot10^{-6}$ cm^2 s^{-1}.

The change in potential induced by the current pulse (ΔE_{PULSE} , without *IR* contributions) can be calculated using equations (2.9) or (2.13). The main difference between these two equations is that equation (2.9) is derived considering that the change in potential is proportional to the change in concentration, whereas

equation (2.13) is based on the Nernst equation. Both equations use the same approach (i.e. equation 2.2) to calculate changes in surface concentration induced by current pulses. Figure 8 compares the experimental response with calculated values for a few pulses (pulses 2, 30 and 70). The values are plotted against $\sqrt{t}$ because this plot would be linear (at least at intermediate times) if the change in potential was proportional to the change in concentration. It is clearly observed that the plots are not linear, except in the case of intermediate pulse numbers (in the present case, for pulses between 20 and 40, corresponding to SOC between 15% and 35%). Deviations between the experimental data and calculations using equation (2.9) are obvious, due to the fact that the changes in potential and concentration are not proportional, except for intermediate pulse numbers. The calculations using equation (2.13) give a better agreement with the experimental data, but still some deviations are clearly visible which can be attributed to some simplifications in the calculations (for example, trace amounts of EtV^+ might be present initially in the cell).

For intermediate pulse numbers, it is possible to make a linear fit of ΔE_{PULSE} vs. $\sqrt{t}$ in the region where the plot is reasonably linear, as illustrated in figure 9. With that, the slope of the plot can be used to evaluate the diffusion coefficient using equation (2.12). For other pulse numbers, the plot is non-linear. In that case, one can take the total change in potential induced by the pulse, without IR contributions, as illustrated in figure 9, and use that value to calculate the diffusion coefficient using equation (2.11). This latter approach is equivalent to forcing a linear fit to a plot that is not truly linear. For the correction of *IR* effects, we have considered that the resistance of the cell should not depend on the state of charge, since the reduction of EtV^{2+} does not lead to formation of any insoluble products. Therefore, the resistance has been evaluated for pulses that show the expected linear behavior of ΔE_{PULSE} vs. $\sqrt{t}$ at longer times, when the *IR* drop formation is complete (see figure 9, which shows R = 168 Ω), and we have considered the same value of resistance for all the pulses.

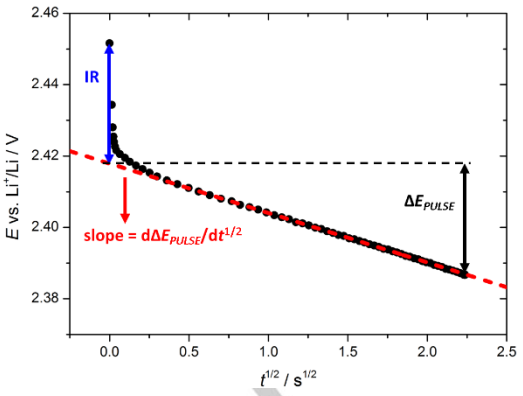

Figure 9. Illustration of how the values of ΔE_{PULSE} and $d\Delta E_{PULSE}/\sqrt{t}$ have been obtained for one pulse in GITT data (pulse 30) for the evaluation of the diffusion coefficient in figure 10.

Figure 10 compares the evaluation of the diffusion coefficient from GITT data using equations (2.11) and (2.12) and from voltammetric data using equation (1.1). A marked variation of the value of the diffusion coefficient with the state of charge is observed upon application of equation (2.11), and also equation (2.12) but to a smaller extent. The cause for these unrealistic variations is illustrated in figure 11, where the equilibrium potential (as obtained from the rest potential in GITT measurements) is plotted vs. concentration (where concentrations are calculated using Faraday's law). For the present GITT experiments, the change in surface concentration induced by each current pulse is ca. 1.7 mM at the end of the pulse (see equation (2.6) and figure 4). On the other hand, the change in the bulk concentration, which is reached at the end of the relaxation state, is only 0.04 mM. Therefore, the change in surface concentration, and corresponding change in potential, at the end of each current pulse is equivalent to the change in bulk concentration, and corresponding change in equilibrium potential, attained by ca 1.7/0.04 = 42 pulses. This is illustrated by the arrows or "pulse trajectories" in figure 11, for pulses 2, 30 and 70.

According to equations (2.5) and (2.7), the change in potential during the current pulse should be proportional to the change in surface concentration, and likewise the change in equilibrium potential should be proportional to the change in bulk concentration. Moreover, the proportionality constant should be the same for both cases. In other words, for each pulse, the gradient dE_{PULSE}/dc_{PULSE} should be equal to the gradient dE_{RELAX}/dc_{BULK}. Visually, this condition requires that the "trajectories" illustrated in figure 11 span a region where the variation of potential with concentration is linear and overlaps with the arrow. In view of figure 11, it is clear that only for pulse 30 is this true. For the other pulses, $d\Delta E_{RELAX} / \Delta c_{RELAX}$ (i.e. the variation of equilibrium potential with bulk concentration) is greater than $d\Delta E_{PULSE} / \Delta c_{PULSE}$ (i.e. the variation of pulse potential with surface concentration) for the first pulses, and it is less than $d\Delta E_{PULSE} / \Delta c_{PULSE}$ for the latest pulses. Thus the classical GITT analysis produces an overestimation of the diffusion coefficient for the first pulses, and an underestimation for the latest pulses.

In conclusion, it is essential to check the condition of potential-concentration linearity in order to validate the results of the evaluation of diffusion coefficients using GITT. This can be done as follows. First, a plot of equilibrium potential vs. bulk concentration can be made, as illustrated in figure 11. Alternatively, if the evaluation of bulk concentration is uncertain, the analysis can be done by plotting potential vs. pulse number, for example. Then, by reference to this curve, an arrow or "trajectory" for each pulse can be drawn, even where the change in surface concentration induced by the pulse cannot be calculated (which, indeed, will normally be the case, since equation (2.6) requires prior knowledge of the diffusion coefficient). The displacement in the y-axis of the "trajectory", is simply defined by the change in potential at the end of the pulse (that is, the value of ΔE_{PULSE} at t = τ, without *IR* effects), and the corresponding displacement in the x-axis can then be found by using the experimental potential vs. pulse number curve. If the trajectory occurs within a region where the potential varies linearly with pulse number, then the evaluation of the diffusion coefficient is reliable. It should also be noted that the precision in the evaluation of the diffusion coefficient is probably limited to an order of magnitude estimation, since, as in many other electrochemical techniques, the value of the diffusion coefficient depends on the square of a combination of experimental values, and hence uncertainities in the experimental data are amplified.

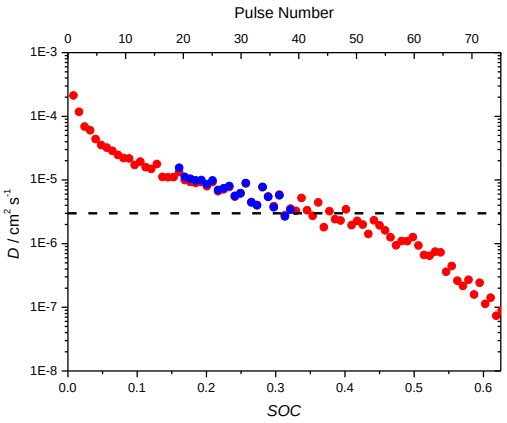

Figure 10. Diffusion coefficient of ethyl viologen as evaluated from GITT data applying equation 2.11 (red points) or equation 2.12 (blue points) and voltammetric data (black dashed line, using equation 1.1).

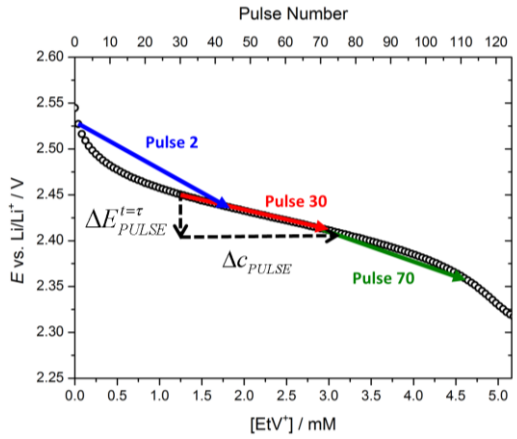

Figure 11. Plot of equilibrium potential vs. EtV^{2+} bulk concentration, and arrows illustrating the changes in potential and concentration induced by pulses 2,30 and 70. The graph also illustrates the strategy to draw trajectories when only $\Delta E_{PULSE}^{t=\tau}$ is known experimentally.

Conclusions

GITT is a powerful tool to evaluate the transport kinetics of species in complex media. Advantages with respect to other electrochemical techniques, such as cyclic voltammetry, include the fact that GITT can provide an evaluation of the diffusion coefficient without any knowledge about the number of electrons or concentration of the species (equations 2.11 and 2.12). However, the analysis of GITT data should be done with care, since unrealistic values of diffusion coefficient can be obtained if the assumptions behind the classical analysis proposed by Weppner and Huggins[1] are not fulfilled. In particular, the condition of proportionality between potential and concentration is difficult to meet experimentally and often neglected. In this work, we provide a rigorous testing of the approach using a well-behaved electrochemical system, we demonstrate that the analysis of GITT data can provide a reliable evaluation of the diffusion coefficient, and we propose a method to validate the result, which requires only the experimental rest potentials obtained in the same GITT measurements.

Experimental Section

For the electrolytes, ethyl viologen triflate ($EtV(OTf)_2$) was prepared in-house according to the literature[81] from ethyl viologen di-iodide ($EtVI_2$, 99%, Sigma-Aldrich) and silver triflate (AgOTf, ≥99%, Sigma-Aldrich). 1,3-dioxolane (Sigma-Aldrich, 99.8% purity, anhydrous) and lithium bis(trifluoromethane)-sulfonamide salt (LiTFSI) (99.95%, Sigma-Aldrich) were dried and deoxygenated under vacuum at 120 °C for 24 hours. The electrolytes (1 M LiTFSI in 1-3 dioxolane with and without 5 mM $EtV(OTf)_2$ were prepared inside an argon filled glovebox (< 1 ppm water content, < 10 ppm oxygen content, M-Braun). Cells were assembled inside the same glovebox.

The cell used for cyclic voltammetry is shown in Figure 12. A glassy carbon working electrode or 'probe' (3 mm diameter, type 2, Alfa Aesar) is embedded in a 1-inch diameter glass disc attached to a glass tube. A thin copper rod in contact with the back face of the glassy carbon serves as the current collector. Prior to use, the glassy carbon electrode was polished with 25, 3.0 and 0.3 µm alumina powder in deionised water and dried under vacuum at 80 °C for a minimum of 30 minutes. $Li_{0.5}FePO_4$ electrodes were prepared by mixing $LiFePO_4$ (battery grade, Tatung), $FePO_4$ (prepared in-house by delithiating $LiFePO_4$)[82], carbon black (acetylene, 100% compressed, Chevron Philips) and PTFE (6CN, DuPont) in the ratio 4:4:1:4 (wt%) in a pestle and mortar. The composite material was roll-pressed to a thickness of 100 µm and punched to a required diameter of 12 mm. $Li_{0.5}FePO_4$ electrodes and glass fibre separators (GF/F, Whatman, 350 µm thickness, punched to 12 mm diameter) were dried under vacuum at 120 °C for 24 hours. Three separators and 150 µL of electrolyte were used for each cell.

The cell used for GITT measurements is shown in Figure 13. The cell comprised (in order) a lithium metal negative electrode (25 mm diameter), one glass-fibre separator (GF/F, Whatman, 350 µm thickness, punched to 25 mm diameter, dried) soaked with 1 M LiTFSI in DOL electrolyte (0.25 mL), a piece of lithium ion conducting glass-ceramic (Ohara Corporation, 1 inch diameter, 150 µm thickness, rinsed with acetone and dried under vacuum at 80 °C overnight), two glass-fibre separators (GF/F, Whatman, 350 µm thickness, punched to 18 mm diameter, dried) soaked with 5 mM $EtV(OTf)_2$ in 1 M LiTFSI in DOL electrolyte (0.25 mL), and a carbon-coated aluminium foil positive electrode (15 mm diameter, 1.5-2 µm coating thickness, dried under vacuum at 120 °C for 24 hours).

All electrochemical measurements were carried out using a Bio-logic VMP2 variable multichannel potentiostat/galvanostat controlled by EC Lab software. All measurements were carried out at a controlled (external) temperature of 25 °C.

For the cyclic voltammetry (CV) measurements, scan rates of 200, 150, 100, 70, 50 and 20 mV s^{-1} were applied. Cells were allowed to rest for 2 hours at 25 °C before commencing the experiments. Prior to each scan rate, cells were held at 3.25 V vs Li^+/Li for 15 minutes to ensure 100% concentration of EtV^{2+}. The potential was then scanned to 2.2 V vs Li^+/Li, and back to 3.25 V vs Li^+/Li. Two cycles per scan rate were measured (results presented are from the first cycle). Measurements were done using ECLab's 'manual IR compensation' function, which automatically applies a *IR* correction during the measurements, using a manually-inputted value of resistance of 150 Ω, as obtained from the high frequency intercept in impedance measurements, and a correction factor of 80%.

For the GITT measurements, the open circuit potential was measured for 60 minutes, followed by 5 seconds of discharge at 0.2 mA (0.11 mA cm^{-2}), then 60 minutes of rest and so on. During the current pulse, data points were recorded every 1 mV or 0.1 s; during the rest period, data points were recorded every 1 mV or 600 s.

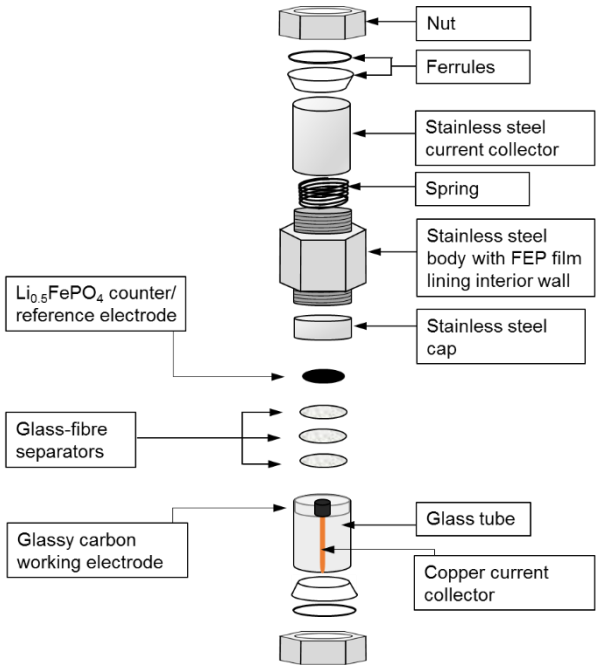

Figure 12. Sketch of Swagelok cell with glassy carbon electrode used for cyclic voltammetry.

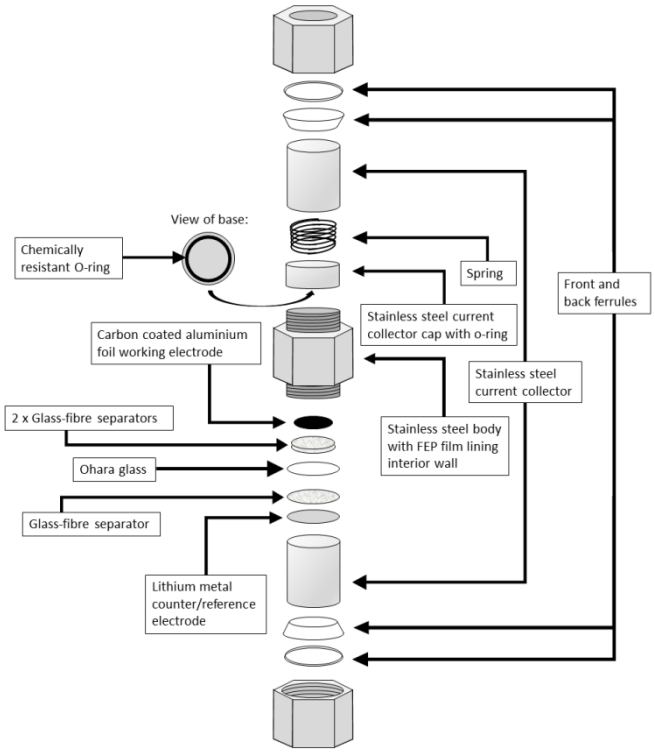

Figure 13. Sketch of Swagelok cell used for GITT measurements.

Acknowledgements

The authors acknowledge financial support from EPSRC and Innovate UK through the MESS project in collaboration with Oxis Energy Ltd. (EP/P019099/1). JWD acknowledges Oxis Energy Ltd., the University of Southampton and EPSRC (EP/M50662X/1) for a CASE studentship. NM acknowledges EPSRC (EP/L016818/1) and the CDT in Energy Storage and its Applications for a studentship. NGA acknowledges EPSRC (EP/N024303/1) for an early career fellowship.

Keywords: diffusion coefficient; Galvanostatic Intermittent Titration Technique (GITT); lithium-sulfur batteries

References:

[1] W. Weppner, R. A. Huggins, *J. Electrochem. Soc.* **1997**, *124*, 1569-1578.
[2] M. J. Lacey, *ChemElectroChem* **2017**, *4*, 1997-2004.
[3] M. J. Lacey, K. Edstrom, D. Brandell, *Chem. Commun.* **2015**, *51*, 16502-16505.
[4] M. R. Busche, P. Adelhelm, H. Sommer, H. Schneider, K. Leitner, J. Janek, *J. Power Sources* **2014**, *259*, 289-299.
[5] M. Cuisinier, P. E. Cabelguen, B. D. Adams, A. Garsuch, M. Balasubramanian, L. F. Nazar, *Energy Environ. Sci.* **2014**, *7*, 2697-2705.
[6] J.-W. Park, K. Yamauchi, E. Takashima, N. Tachikawa, K. Ueno, K. Dokko, M. Watanabe, *J. Phys. Chem. C* **2013**, *117*, 4431-4440.
[7] S. Waluś, C. Barchasz, R. Bouchet, J. F. Martin, J. C. Leprêtre, F. Alloin, *Electrochim. Acta* **2015**, *180*, 178-186.
[8] J.-J. Kim, H. S. Kim, J. Ahn, K. J. Lee, W. C. Yoo, Y.-E. Sung, *J. Power Sources* **2016**, *306*, 617-622.
[9] S.D. Talian, J. Moškon, R. Dominko, M. Gaberšček *ACS Appl. Mater. Interfaces* **2017**, *9*, 29760−29770.
[10] V.S. Kolosnitsyn, E.V. Kuzmina, S.E. Mochalov, *J. Power Sources* **2014**, *252*, 28-34.
[11] V.S. Kolosnitsyn, E.V. Kuzmina, E.V. Karaseva, S.E. Mochalov, *J. Power Sources* **2011**, *196*, 1478-1482.
[12] L. Yuan, X. Qiu, L. Chen, W. Zhu, *J. Power Sources* **2009**, *189*, 127-132.
[13] N.A. Cañas, K. Hirose, B. Pascucci, N. Wagner, K.A. Friedrich, R. Hiesgen, *Electrochim. Acta* **2013**, *97*, 42-51.
[14] Y. Li, H. Zhan, S. Liu, K. Huang, Y. Zhou, J. Power Sources 2010, 195, 2945-2949.
[15] C. Barchasz, J.-C. Leprêtre, F. Alloin, S. Patoux, J. Power Sources 2012, 199, 322-330.
[16] T. Zhang, M. Marinescu, L. O'Neill, M. Wild, G. Offer, *Phys.Chem.Chem.Phys.* **2015**, *17*, 22581-22586.
[17] T. Zhang, M. Marinescu, S. Walus, P. Kovacik, G.J. Offer, *J. Electrochem. Soc.* **2018**, *165 (1)*, A6001-A6004.
[18] S. Risse, N.A. Cañas, N. Wagner, E. Härk, M. Ballauff, K.A. Friedrich, J. Power Sources, 2016, 323, 107-114.
[19] Z. Deng, Z. Zhang, Y. Lai, J. Liu, J. Li, Y. Liu, J. Electrochem. Soc. 2013, 160 (4), A553−A558.
[20] A. Ganesan, A. Varzi, S. Passerini, M.M. Shaijumon, Electrochim. Acta 2016, 214, 129−138.
[21] K.H. Wujcik, T.A. Pascal, C.D. Pemmaraju, D. Devaux, W.C. Stolte, N.P. Balsara, D. Prendergast, *Adv. Energy Mater.* **2015**, *5*, 1500285.
[22] M.A. Lowe, J. Gao, H.D. Abruna, *RSC Adv.* **2014**, *4*, 18347-18353.
[23] Y. Gorlin, A. Siebel, M. Piana, T. Huthwelker, H. Jha, G. Monsch, F. Kraus, H. A. Gasteiger, M. Tromp, *J. Electrochem. Soc.* **2015**, *162*, A1146−A1155.

[24] M. Cuisinier, P. E. Cabelguen, B. D. Adams, A. Garsuch, M. Balasubramanian, L. F. Nazar, *Energy Environ. Sci.* **2014**, *7*, 2697-2705.

[25] M. Cuisinier, P.-E. Cabelguen, S. Evers, G. He, M. Kolbeck, A. Garsuch, T. Bolin, M. Balasubramanian, L. F. Nazar, *J. Phys. Chem. Lett.* **2013**, *4*, 3227-3232.

[26] M. Cuisinier, C. Hart, M. Balasubramanian, A. Garsuch, L. F. Nazar, *Adv. Energy Mat.* **2015**, *5*, 1401801.

[27] M. U. M. Patel, I. Arcon, G. Aquilanti, L. Stievano, G. Mali, R. Dominko, *ChemPhysChem* **2014**, *15 (5)*, 894-904.

[28] X. Feng, M.-K. Song, W. C. Stolte, D. Gardenghi, D. Zhang, X. Sun, J. Zhu, E. J. Cairns, J. Guo, *Phys.Chem.Chem.Phys* **2014**, *16*, 16931-16940.

[29] T. A. Pascal, K. H. Wujcik, J. Velasco-Velez, C. Wu, A. A. Teran, M. Kapilashrami, J. Cabana, J. Guo, M. Salmeron, N. Balsara, D. Prendergast, *J. Phys. Chem. Lett.* **2014**, *5*, 1547-1551.

[30] M. Vijayakumar, N. Govind, E.Walter, S. D. Burton, A. Shukla, A. Devaraj, J. Xiao, J. Liu, C. Wang, A. Karim, S. Thevuthasan, *Phys.Chem.Chem.Phys* **2014**, *16*, 10923-10932.

[31] K. H. Wujcik, J. Velasco-Velez, C. H. Wu, T. Pascal, A. A. Teran, M. A. Marcus, J. Cabana, J. Guo, D. Prendergast, M. Salmeron, N. P. Balsara, *J. Electrochem. Soc.* **2014**, *161*, A1100-A1106.

[32] K.H. Wujcik, D.R. Wang, T.A. Pascal, D. Prendergast, N.P. Balsara, *J. Electrochem. Soc.* **2017**, *164 (2)*, A18-A27.

[33] Y. Sun, Z.W. Seh, W. Li, H. Yao, G. Zheng, Y. Cui, *Nano Energy* **2015**, *11*, 579-586.

[34] M. U. M. Patel, R. Dominko, *ChemSusChem* **2014**, *7*, 2167–2175.

[35] M. U. M. Patel, R. Demir-Cakan, M. Morcrette, J.-M. Tarascon, M. Gaberscek, R. Dominko, *ChemSusChem* **2013**, *6*, 1177–1181.

[36] Q. Zou, Y.-C. Lu, *J. Phys. Chem. Lett.* **2016**, *7*, 1518–1525.

[37] H. Marceau, C.-S. Kim, A. Paolella, S. Ladouceur, M. Lagacé, M. Chaker, A. Vijh, A. Guerfi, C. M. Julien, A. Mauger, et al., *J. Power Sources* **2016**, *319*, 247–254.

[38] N. A. Cañas, D. N. Fronczek, N. Wagner, A. Latz, K. A. Friedrich, *J. Phys. Chem. C* **2014**, *118*, 12106–12114.

[39] C. Barchasz, F. Molton, C. Duboc, J.-C. Leprêtre, S. Patoux, F. Alloin, *Anal. Chem.* **2012**, *84*, 3973–3980.

[40] K. H. Wujcik, D. R. Wang, A. Raghunathan, M. Drake, T. A. Pascal, D. Prendergast, N. P. Balsara, *J. Phys. Chem. C* **2016**, *120*, 18403–18410.

[41] N. Xu, T. Qian, X. Liu, J. Liu, Y. Chen, C. Yan, Nano Lett. 2017, 17, 538–543.

[42] R. Dominko, M. U. M. Patel, V. Lapornik, A. Vizintin, M. Koželj, N. N. Tušar, I. Arčon, L. Stievano, G. Aquilanti, *J. Phys. Chem. C* **2015**, *119*, 19001–19010.

[43] J. Xiao, J. Z. Hu, H. Chen, M. Vijayakumar, J. Zheng, H. Pan, E. D. Walter, M. Hu, X. Deng, J. Feng, et al., *Nano Lett.* **2015**, *15*, 3309–3316.

[44] L. A. Huff, J. L. Rapp, J. A. Baughman, P. L. Rinaldi, A. A. Gewirth, *Surf. Sci.* **2015**, *631*, 295–300.

[45] K. A. See, M. Leskes, J. M. Griffin, S. Britto, P. D. Matthews, A. Emly, A. Van der Ven, D. S. Wright, A. J. Morris, C. P. Grey, et al., *J. Am. Chem. Soc.* **2014**, *136*, 16368–16377.

[46] H. Wang, N. Sa, M. He, X. Liang, L. F. Nazar, M. Balasubramanian, K. G. Gallagher, B. Key, *J. Phys. Chem. C* **2017**, *121*, 6011–6017.

[47] Q. Wang, J. Zheng, E. Walter, H. Pan, D. Lv, P. Zuo, H. Chen, Z. D. Deng, B. Y. Liaw, X. Yu, et al., *J. Electrochem. Soc.* **2015**, *162*, A474–A478.

[48] J. Conder, R. Bouchet, S. Trabesinger, C. Marino, L. Gubler, C. Villevieille, *Nat. Energy* **2017**, *2*, 17069.

[49] G. Tonin, G. Vaughan, R. Bouchet, F. Alloin, M. Di Michiel, L. Boutafa, J.-F. Colin, C. Barchasz, *Sci. Rep.* **2017**, *7*, 2755.

[50] N. A. Cañas, S. Wolf, N. Wagner, K. A. Friedrich, J. Power Sources 2013, 226, 313–319.

[51] S. Walus, C. Barchasz, J.-F. Colin, J.-F. Martin, E. Elkaim, J.-C. Lepretre, F. Alloin, *Chem. Commun.* **2013**, *49*, 7899–7901.

[52] S. Waluś, C. Barchasz, R. Bouchet, J.-C. Leprêtre, J.-F. Colin, J.-F. Martin, E. Elkaïm, C. Baehtz, F. Alloin, *Adv. Energy Mater.* **2015**, *5*, 1500165.

[53] J.-T. Yeon, J.-Y. Jang, J.-G. Han, J. Cho, K. T. Lee, N.-S. Choi, *J. Electrochem. Soc.* **2012**, *159*, A1308–A1314.

[54] W. Zhu, A. Paolella, C.-S. Kim, D. Liu, Z. Feng, C. Gagnon, J. Trottier, A. Vijh, A. Guerfi, A. Mauger, et al., Sustain. Energy Fuels 2017, 1, 737–747.

[55] J. Nelson, S. Misra, Y. Yang, A. Jackson, Y. Liu, H. Wang, H. Dai, J. C. Andrews, Y. Cui, M. F. Toney, *J. Am. Chem. Soc.* **2012**, *134*, 6337–6343.

[56] H.-L. Wu, L. A. Huff, A. A. Gewirth, *ACS Appl. Mater. Interfaces* **2015**, *7*, 1709–1719.

[57] J. McBrayer, T. E. Beechem, B. R. Perdue, F. H. Garzon, C. A. Apblett, *Meet. Abstr.* **2017**, *MA2017-01*, 512.

[58] J. Hannauer, J. Scheers, J. Fullenwarth, B. Fraisse, L. Stievano, P. Johansson, *ChemPhysChem* **2015**, *16*, 2755–2759.

[59] P. Partovi-Azar, T. D. Kuhne, P. Kaghazchi, *PCCP* **2015**, *17*, 22009-22014.

[60] M. Hagen, P. Schiffels, M. Hammer, S. Dörfler, J. Tübke, M. J. Hoffmann, H. Althues, S. Kaskel, *J. Electrochem. Soc.* **2013**, *160*, A1205-A1214.

[61] D. Zheng, D. Liu, J. B. Harris, T. Ding, J. Si, S. Andrew, D. Qu, X.-Q. Yang, D. Qu, *ACS Appl. Mater. Interfaces* **2017**, *9*, 4326–4332.

[62] D. Zheng, D. Qu, X.-Q. Yang, X. Yu, H.-S. Lee, D. Qu, *Adv. Energy Mater.* **2015**, *5*, 1401888.

[63] N. Azimi, Z. Xue, I. Bloom, M. L. Gordin, D. Wang, T. Daniel, C. Takoudis, Z. Zhang, *ACS Appl. Mater. Inter.* **2015**, *7*, 9169-9177.

[64] D. Zheng, X. Zhang, J. Wang, D. Qu, X. Yang, D. Qu, *J. Power Sources* **2016**, *301*, 312-316.

[65] A. Jozwiuk, B. B. Berkes, T. Weiß, H. Sommer, J. Janek, T. Brezesinski, *Energy Environ. Sci.* **2016**, *9*, 2603–2608.

[66] Y.-C. Lu, Q. He, H. A. Gasteiger, *J. Phys. Chem. C* **2014**, *118*, 5733–5741.

[67] M. Safari, C. Y. Kwok, L. F. Nazar, *ACS Cent. Sci.* **2016**, *2*, 560–568.

[68] Y. Cui, Y. Fu, *J. Power Sources* **2015**, *286*, 557–560.

[69] F.Y. Fan, W.C. Carter, Y.-M. Chiang, *Adv. Mater.*, **2015**, *27*, 5203-5209.

[70] Y.V. Mikhaylik, J.R. Akridge, *J. Electrochem. Soc.* **2004**, *151 (11)*, A1969-A1976.

[71] D. Moy, A. Manivannan, S. R. Narayanan, *J. Electrochem. Soc.* **2015**, *162 (1)*, A1-A7.

[72] A.F. Hofmann, D.N. Fronczek, W.G. Bessler, *J. Power Sources* **2014**, *259*, 300-310.

[73] S.M. Al-Mahmoud, J.W. Dibden, J.R. Owen, G. Denuault, N. Garcia-Araez, *J. Power Sources* **2016**, *306*, 323-328.

[74] K. Kumaresan, Y. Mikhaylik, R.E. White, *J. Electrochem. Soc.* **2008**, *155 (8)*, A576-A582.

[75] D.N. Fronczek, W.G. Bessler, *J. Power Sources* **2013**, *244*, 183-188.

[76] M. Ghaznavi, P. Chen, *J. Power Sources* **2014**, *257*, 394-401.

[77] M. Ghaznavi, P. Chen, *J. Power Sources* **2014**, *257*, 402-411.

[78] M. Ghaznavi, P. Chen, *Electrochim. Acta* **2014**, *137*, 575-585.

[79] A.J. Bard, L.R. Faulkner, *Electrochemical Methods: Fundamentals and Applications*, Wiley, New York, **2001**, chapter 8.

[80] N. Meddings, J.R. Owen. N. Garcia-Araez, *J. Power Sources* **2017**, *364*, 148-155.

[81] N. Intaranont, N. Garcia-Araez, A. L. Hector, J. A. Milton and J. R. Owen, Selective lithium extraction from brines by chemical reaction with battery materials, *J. Mater. Chem. A* **2014**, *2*, 6374-6377.

[82] L. Yang, J.T. Frith, N. Garcia-Araez, J.R. Owen, A new method to prevent degradation of lithium-oxygen batteries: reduction of superoxide by viologen, *Chem. Commun.* **2015**, *51*, 1705-8.

Entry for the Table of Contents (Please choose one layout)

Layout 1:

ARTICLE

We provide equations for extracting from GITT measurements the value of the diffusion coefficient of soluble species whose concentration is unknown, such as soluble sulfur and polysulfides in lithium-sulfur batteries. The approach can also be applied to ion-insertion electrodes, where non-linearity of concentration and voltage changes would produce unrealistic evaluations of the diffusion coefficient by the classical analysis of GITT data.

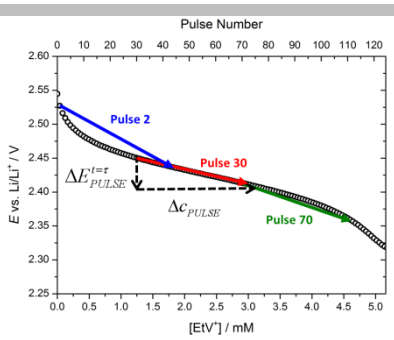

*James W. Dibden, Nina Meddings, John R. Owen and Nuria Garcia-Araez**

Page No. – Page No.

Quantitative GITT analysis for lithium-sulfur batteries: validation with a model system